Molecular Vision 2021; 27:95-106 <http://www.molvis.org/molvis/v27/95>
Received 21 October 2020 | Accepted 16 March 2021 | Published 18 March 2021

Noncoding mutation in *RPGRIP1* contributes to inherited retinal degenerations

Gang Zou,[1,2] Tao Zhang,[2] Xuesen Cheng,[2] Austin D. Igelman,[3] Jun Wang,[2] Xinye Qian,[2] Shangyi Fu,[2] Keqing Wang,[2] Robert K. Koenekoop,[4] Gerald A. Fishman,[5] Paul Yang,[3] Yumei Li,[2] Mark E. Pennesi,[3] Rui Chen[2]

[1]Department of Ophthalmology, Ningxia Eye Hospital, People's Hospital of Ningxia Hui Autonomous Region, First Affiliated Hospital of Northwest University for Nationalities, Ningxia Clinical Research Center on Diseases of Blindness in Eye, Yinchuan, China; [2]Human Genome Sequencing Center, Baylor College of Medicine, Houston, Texas; [3]Department of Ophthalmology, Casey Eye Institute, Oregon Health & Science University, Portland, Oregon; [4]Department of Paediatric Surgery, Human Genetics and Adult Ophthalmology, MUHC, Montréal, Quebec, Canada; [5]Pangere Center for Inherited Retinal Diseases, The Chicago Lighthouse, Chicago, IL

Purpose: Despite the extensive use of next-generation sequencing (NGS) technology to identify disease-causing genomic variations, a major gap in our understanding of Mendelian diseases is the unidentified molecular lesion in a significant portion of patients. For inherited retinal degenerations (IRDs), although currently close to 300 disease-associated genes have been identified, the mutations in approximately one-third of patients remain unknown. With mounting evidence that noncoding mutations might contribute significantly to disease burden, we aimed to systematically investigate the contributions of noncoding regions in the genome to IRDs.

Methods: In this study, we focused on *RPGRIP1*, which has been linked to various IRD phenotypes, including Leber congenital amaurosis (LCA), retinitis pigmentosa (RP), and macular dystrophy (MD). As several noncoding mutant alleles have been reported in *RPGRIP1,* and we observed that the mutation carrier frequency of *RPGRIP1* is higher in patient cohorts with unsolved IRDs, we hypothesized that mutations in the noncoding regions of *RPGRIP1* might be a significant contributor to pathogenicity. To test this hypothesis, we performed whole-genome sequencing (WGS) for 25 patients with unassigned IRD who carry a single mutation in *RPGRIP1.*

Results: Three noncoding variants in *RPGRIP1*, including a 2,890 bp deletion and two deep-intronic variants (c.2710+233G>A and c.1468–263G>C), were identified as putative second hits of *RPGRIP1* in three patients with LCA. The mutant alleles were validated with direct sequencing or in vitro assays.

Conclusions: The results highlight the significance of the contribution of noncoding pathogenic variants to unsolved IRD cases.

The most common cause of hereditary blindness around the world is inherited retinal degenerations (IRDs), a group of Mendelian disorders that are clinically and genetically heterogeneous. In the past decade, advancements in next-generation sequencing technologies have greatly improved the molecular diagnostic rate for patients with IRDs [1-4]. However, currently about one-third of the underlying pathogenic mutations in patients with IRDs remain unassigned, representing one of the major gaps in the field [1]. Recent studies have shown that mutations outside coding exons could be a significant contributor to the disease. For example, one of the most frequently observed mutations in patients with Leber congenital amaurosis (LCA) is an intronic mutation (c.2991+1655A→G) in *CEP290* (Gene ID: 80184; OMIM: 610142), which creates a common splice-donor site in an intron and leads to the inclusion of a cryptic exon [5-8]. Similarly, multiple deep-intronic mutations that can lead to cryptic mRNA splicing have been identified in *ABCA4* (Gene ID: 24; OMIM: 601691) [9-17]. Several of these near- or deep-intronic variants in *ABCA4* were shown to lead to a frame shift that results in the formation of a premature stop codon, leading to a subsequent, predicted protein change or disruption of mRNA splicing [18]. In addition to deep-intronic mutations, chromosomal structure mutations have been observed in patients with IRDs. For example, deletions and duplications are frequently observed in *USH2A* (Gene ID: 7399; OMIM: 608400) [19,20]. Therefore, systematically screening mutations across the genomic loci might reveal pathogenic mutations for a significant portion of patients who remain unassigned after exon sequencing technology.

A commonly mutated gene in patients with IRDs is *retinitis pigmentosa GTPase regulator interaction protein 1* (*RPGRIP1*; Gene ID: 57096; OMIM: 605446) [21]. Mutations in *RPGRIP1* have been associated with a range of inherited retinal diseases, such as retinitis pigmentosa (RP), and cone rod dystrophy (CRD) [22-26]. *RPGRIP1*, which is located

Correspondence to: Rui Chen, Human Genome Sequencing Center Baylor College of Medicine, Room N1519, One Baylor Plaza, Houston, Texas, 77030; Phone: (713) 798-5194; FAX: (713) 798-5741; email: ruichen@bcm.edu

on the long arm of the chromosome 14 (14q11.2), is a large gene that spans 63 Kb and contains 24 exons, which encode a 1,286 amino acid protein (nucleotide accession number: NM_020366.3). RPGRIP1 plays an important role in the connecting cilium of photoreceptor cells, which is critical for controlling protein trafficking between the inner segment and the outer segment of the photoreceptors. Directly binding to RPGR and SPATA7, RPGRIP1 functions in the RPGR complex, which is important for proper localization of other cilia transition zone complexes, such as the transport of the nephronophthisis (NPHP) protein complex to the connecting cilium in photoreceptor cells [27-31].

Currently, various types of likely pathogenic alleles in *RPGRIP1* have been observed, including missense, splicing, deletion, duplication, and frameshift alterations in human gene mutation database (HGMD). Rare, noncoding, and complex mutations in *RPGRIP1* have also been reported, including a homozygous deletion in exon 17 of the gene [32]. Additionally, structural variations and deep-intronic mutations have been reported in *RPGRIP1*, suggesting that these complex and noncoding mutations may contribute significantly to the mutation load [33].

To assess the contribution of mutations in *RPGRIP1* that are missed by coding exon capture sequencing, we examined mutations in *RPGRIP1* in a cohort of 762 patients with RP and 171 patients with LCA whose mutations have not been found. Among them, we identified 15 patients with RP and ten patients with LCA carrying one likely pathogenic mutation in the coding exons of *RPGRIP1*, (i.e., patients with one hit in *RPGRIP1*). The carrier mutation frequency in *RPGRIP1* in the general population is calculated based on the Genome Aggregation Database (gnomAD) for LCA and RP as described previously [34]. Compared to the control population, the number of patients with one hit in *RPGRIP1* was significantly higher in the patient cohort with LCA than expected (expected 1.35%, observed 5.85%, p=1.26E-04), while the number of patients in the patient cohort with RP with one hit in *RPGRIP1* was not significantly higher (expected 1.95%, observed 1.97%, p=0.52). To identify putative noncoding mutations in these patients with one hit in *RPGRIP1*, a combination of short and 10X genomics linked read whole genome sequencing (lrWGS) was performed. As a result, three noncoding variants in *RPGRIP1*, including one large deletion and two deep-intronic variants, were identified as putative mutations. The deletion allele spans 2,890 bp in length, uncovering exon 21 and resulting in a frameshift mutation and a premature stop codon. In vitro minigene splicing assay of the two deep-intronic variants (c.2710+233G>A and c.1468–263G>C) supported that these two variants affect proper splicing and lead to the inclusion of cryptic exons.

METHODS

Ethical guidelines and patient recruitment: The study was approved by the Department of Molecular and Human Genetics, Baylor College of Medicine, and adhered to the Declaration of Helsinki and to the ARVO Statement on Human Subjects. Written informed consent was obtained from all individuals on whom genetic testing and further molecular evaluations were performed. The pedigree information of all individuals was obtained from Casey Eye Institute Oregon Health & Science University for genetic analysis and further molecular evaluation. Research Ethics Board (REB) approval was obtained by the McGill University Health Centre Research Institute (MUHC RI) ethics board. All patients in this study underwent clinical assessment by experienced ophthalmologists.

DNA sequencing: Blood was collected from each proband and their family members when available after informed consent was obtained. Venous blood samples were obtained from the probands and Genomic DNA was extracted. All DNA samples were stored at -80°C freezer. DNA was extracted using the QIAamp DNA Blood Mini Kit (Qiagen, Hilden, Germany). All patient DNA underwent whole-exome sequencing (WES) and WGS and was further examined at the Human Genome Sequencing Center, Baylor College of Medicine. The Sanger sequencing primer design was as follows: MEP-305: RPGRIP1_112_F: 5′-GTG CCT TTA CTG CCT CTT GC-3′, R: 5′-CAG CAT TAC AGA GCT TGA AAA A-3′; MEP-318: RPGRIP1_113_F: 5′-GTG CAC AGG GAA AAT CCA CT-3′, R: 5′-GCT AAG GTA CTG GAG AAA AAT GC-3′; RKK-665: RKK665_F: 5′-TCC TCC TGG TAT CCC TGA TG-3′, R: 5′-CCT GTG GGT CCA GGT CTA TT-3′.

Bioinformatics analysis: The WGS data were processed using a pipeline modified from our previous WES data analysis pipeline. Briefly, next-generation sequencing (NGS) sequencing reads were aligned to the human genome assembly (hg19) with Burrows-Wheeler aligner (BWA) [35]. Single nucleotide variants and small insertion-deletion variants (SNVs and indels) are identified using genome analysis toolkit (GATK), and structure variants (SVs) and copy number variants (CNVs) are identified using a set of bioinformatics tools, including CNVnator, DELLY, LUMPY, and MANTA. A population allele frequency threshold of 0.5% was applied to filter out common variants based on the allele frequency in the gnomAD database and the center's internal whole genome sequencing databases of 50,000 people without eye diseases. For SNVs, variants that were mapped to the

coding region were annotated with ANNOVAR and searched against the dbNSFP. The conservation of the remaining variants was calculated based on the genomic evolutionary rate profiling (GERP) score. The effect of the variants was predicted using combined annotation dependent depletion (CADD) [36,37]. The deleteriousness of SNVs was predicted using the latest CADD score (score cutoff = 20), which is derived based on more than 60 annotations, including Ensembl Variant Effect Predictor (VEP), The Encyclopedia of DNA Elements (ENCODE), multiple conservation and protein predictions, splicing prediction, and database for nonsynonymous SNPs' functional predictions (dbNSFP) [38]. For SVs and CNVs, variants were annotated to the RefSeq gene database and filtered with the SV and CNV QC tool svtyper (score cutoff = 100) [39,40]. Raw bam files that contained candidate SVs and CNVs were further viewed manually through integrative genomics viewer (IGV) to rule out potential false positive calls from mapping errors or sequencing errors before experimental validation. To predict if the variants might affect splicing, SpliceAI was applied to all the WGS variants of the cases with *RPGRIP1* with one hit (cutoff = 0.2) [41].

Minigene molecular cloning, transfection, and RT–PCR: To assess whether the prioritized variants have an effect on splicing, we used an established minigene reporter assay, the RHCglo minigene [42]. DNA fragments, including 500 bp flanking each side of the putative intronic mutation, were PCR amplified using genomics DNA from the corresponding patient as the template and cloned into the RHCglo minigene vector. PCR amplification consisted of: denaturation step at 95°C for 15 s followed by 40 cycles of 95°C for 30 s, 58°C for 30 s, and 72°C for 1 min/kb, and a final extension step at 72°C for 5 min. The impact of the variant on mRNA splicing was examined by transfecting the plasmid to the human embryonic kidney 293 (HEK293) cell line followed with reverse transcriptase (RT)–PCR as described previously [42]. The HEK293 cell line was validated with short tandem repeat (STR; Appendix 1) profiling.

RESULTS

To identify patients with likely pathogenic mutations in *RPGRIP1*, we first analyzed WES data of 933 IRD cases, including 762 patients with RP and 171 patients with LCA, whose causal mutations were unknown. The analytic procedure for the WES data is shown in a flowchart in Figure 1. As a result, we identified 15 patients with RP and ten patients with LCA who carry a single pathogenic or likely pathogenic variant in *RPGRIP1* (Table 1). Using the same criteria, we screened deleterious variants in *RPGRIP1* in the gnomAD, which was used as the control population, to infer the background carrier frequency of *RPGRIP1*. Based on the inferred background carrier frequency of *RPGRIP1*, we deduced that the expected number of carriers with one hit of *RPGRIP1* in the patient cohort with unsolved LCA was about two or three. However, we observed ten patients with LCA carrying a single likely pathogenic variant in *RPGRIP1* in the cohort, indicating that the observed number of patients with one hit of *RPGRIP1* in the patient cohort with unsolved LCA is significantly higher than expected (Table 2, binomial test, one sided, p=1.26E-04). Similarly, based on the background carrier frequency of *RPGRIP1*, the expected number of carriers with one hit of *RPGRIP1* in the patient cohort with unsolved RP was about 15. However, there were 15 patients with RP carrying a single likely pathogenic variant in *RPGRIP1* in the cohort, suggesting the observed number of carriers of mutations in *RPGRIP1* in the patient cohort with unsolved RP was not significantly higher than expected (Table 2, binomial test, one sided, p=0.52). Overall, these results suggest that it is likely that some of these ten patients with LCA with one hit of *RPGRIP1* might have a second pathogenic allele in *RPGRIP1*. To test this idea, WGS was performed to identify potential mutations in *RPGRIP1* that were missed by previous WES. Candidate structural variants and deep-intronic cryptic splicing mutations were identified by analyzing the WGS data as described in the methods section (Table 3).

We identified in two patients with unsolved LCA two deep-intronic variants that are predicted to affect splicing . Each deep-intronic splicing variant was validated with Sanger sequencing, and the corresponding minigene gel band, which could be cleanly excised, was sequenced to confirm its composition. The RNA extracted from the HEK293 cells was used for RT–PCR. Both gel bands indicated that the mutants produced new bands in contrast to the wild-type patients, both of which are shown in Figure 2.

The first deep-intronic variant was c.2710+233G>A, which is located at chromosome 14 and base position 21,794,565 (hg19) and was predicted to result in the creation of a new splicing donor site. This variant has not been previously described and was found in a patient with LCA, MEP_305, who also carries a c.3793_3794insGAAA (p.(Val1265GlyfsTer19) frameshift mutation (Table 3). To confirm this prediction, intronic DNA fragments containing the variant or the wild-type sequence were cloned into the minigene vector. Both constructs were transfected into the HEK293 cell line and subjected to mRNA splicing assay. As shown in Figure 2, compared to the wild-type control, the variant showed a larger RT–PCR band in the variant construct, indicating the inclusion of a cryptic exon. Sequencing of the

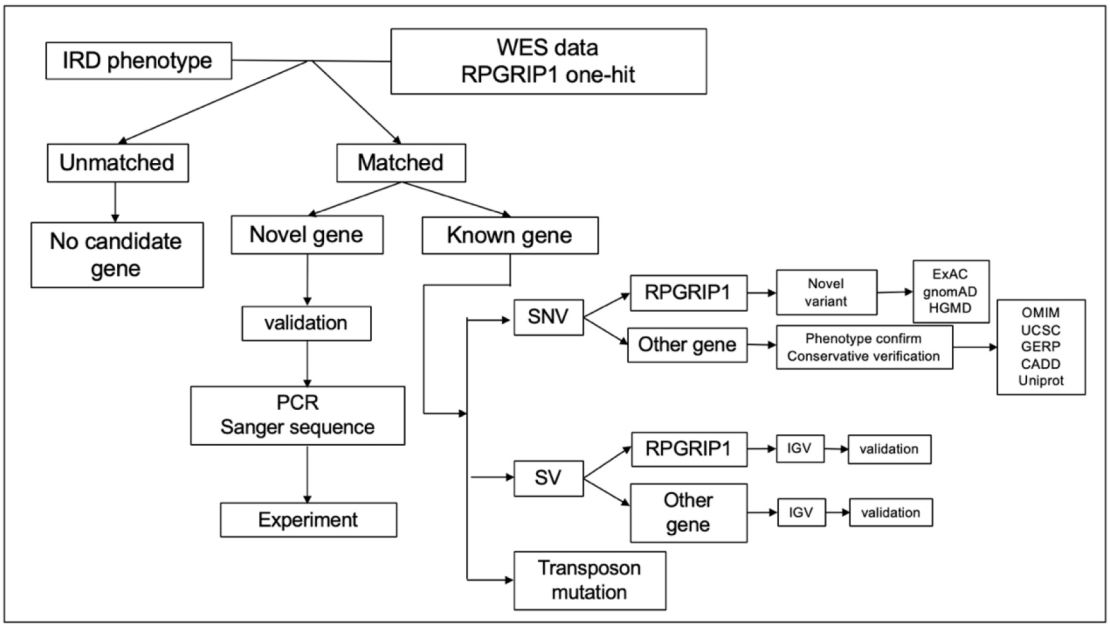

Figure 1. Our data analysis pipeline.

RT–PCR product indicated that the cryptic exon is 134 bp in length spanning chromosome 14 from the base positions 21,794,477 to 21,794,610 (Figure 2).

The second deep-intronic variant was c.1468–263G>C, identified in a patient with LCA, MEP_318, who carries the frameshift insertion c.934dupC (p.(Gln312ProfsTer9)). This intronic variant was described in a previous report [33], in which the variant was predicted to generate a novel splicing donor site. As shown in Figure 2, an extra RT–PCR band that was larger than that observed for the variant construct compared to the wild-type control in the minigene splicing test. Sequencing of the large RT–PCR band revealed that the cryptic exon is 120 bp in length, spanning the base positions 21,789,216 to 21,789,335 on chromosome 14.

Consistent with the molecular mutation in *RPGRIP1*, the clinical phenotypes of both affected individuals showed the typical LCA phenotype (Figure 3A,B). MEP_305 is female, who first presented at age 4 years with congenital nystagmus. At the age of 4 years, the best-corrected visual acuity (BCVA) of her right eye was 20/125, while the BCVA of her left eye was 20/200. At 7 years, her BCVA decreased to 20/400 for both eyes. Fundus examination disclosed moderate waxy pallor of the optic nerves, pigmentary mottling in the macula, as well as moderate vascular attenuation. The pigmentary changes inferiorly are secondary to laser for a Coats-like reaction that the patient developed (Figure 3A, top row). Fundus autofluorescence (FAF) showed peripheral hypo-AF and hyper-AF rings of the parafovea and midperiphery bilaterally (Figure 3A, second row). MEP_318 is male, who presented with congenital nystagmus, photophobia, and poor visual acuity since the age of 2 years. At the age of 2 years, his BCVA was estimated to be 20/1,000 for both eyes. At 8 years, his BCVA decreased to 20/1,600 for the right eye, whereas the left eye was light perception (LP) visual acuity. Fundus examination disclosed vascular attenuation, RPE atrophy with increased visibility of the choroidal vessels, fine granular pigmentation just outside the vessels, and yellow deposits in the periphery (Figure 3B, top row). FAF depicted perimacular hyper-AF ring bilaterally (Figure 3B, second row). Full-field electroretinography (ffERG) for both patients revealed severe cone and rod dysfunction (Figure 3A,B, bottom), and the two patients retained foveal structure on optical coherence tomography (OCT) imaging (Figure 3A,B, third row).

In addition, one deletion was identified in a patient with LCA (RKK_665) who also carries a c.2627A>G (p.(Asp876Gly)) missense mutation (Table 3). The deletion has not been reported previously. As shown in Figure 4A, reduced read coverage and discordant read mate pairs were observed. To confirm the deletion and determine the breakpoint, PCR was performed to amplify the genomic region of the mutant chromosome, and the PCR product was Sanger sequenced. As shown in Figure 4C, a PCR product was obtained using genomic DNA from the patient as the template. Sequencing of the PCR product indicated that the breakpoints are mapped at chromosome 14 and base positions

Table 1. Single mutant alleles in the 25 *RPGRIP1* mutation carriers.

Patient ID	Phenotype	Zygosity	Exon	cDNA variant	Protein variant	gnomAD (Allele frequency)
Known likely pathogenic variant candidates						
1332	LCA	heterozygous	exon14	c.2017C>T	p.(Gln673Ter)	0
3443	LCA	heterozygous	exon16	c.2627A>G	p.(Asp876Gly)	0
RKK_665	LCA	heterozygous	exon16	c.2627A>G	p.(Asp876Gly)	0
Novel likely pathogenic variant candidates						
			Missense variants			
SRF2147	LCA	heterozygous	exon5	c.775T>C	p.(Cys259Arg)	0
3647	LCA	heterozygous	exon16	c.2434C>T	p.(Arg812Trp)	2.41E-05
SRF_1990	RP	heterozygous	exon3	c.416C>T	p.(Ala139Val)	4.82E-06
SRF_436	RP	heterozygous	exon3	c.473C>T	p.(Pro158Leu)	4.98E-06
14,132,001	RP	heterozygous	exon8	c.1015A>G	p.(Lys339Glu)	8.07E-06
SRF_1536	RP	heterozygous	exon14	c.1862T>C	p.(Leu621Pro)	0
SRF_569	RP	heterozygous	exon14	c.2132A>G	p.(His711Arg)	0
SRF_1447	RP	heterozygous	exon15	c.2291C>T	p.(Ala764Val)	2.55E-05
NEI_8	RP	heterozygous	exon16	c.2480G>A	p.(Arg827His)	6.06E-05
4270jyc	RP	heterozygous	exon16	c.2600G>A	p.(Arg867Gln)	7.49E-05
RKK_78	RP	heterozygous	exon16	c.2632G>A	p.(Glu878Lys)	1.79E-05
SRF_841	RP	heterozygous	exon18	c.2965G>A	p.(Gly989Arg)	2.81E-05
SRF_825	RP	heterozygous	exon20	c.3242A>G	p.(Lys1081Arg)	0
			Frameshift variants			
MEP_318	LCA	heterozygous	exon8	c.934dupC	p.(Gln312ProfsTer9)	0
207_3	LCA	heterozygous	exon9	c.1107delA	p.(Glu370AsnfsTer5)	0
SRF_168	LCA	heterozygous	exon14	c.1951delA	p.(Thr651ProfsTer33)	0
MEP_305	LCA	heterozygous	exon24	c.3793_3794insGAAA	p.(Val1265GlyfsTer19)	4.04E-06
WLJ_029	RP	heterozygous	exon5	c.673delC	p.(His225ThrfsTer50)	1.20E-05
SRF_684	RP	heterozygous	exon10	c.1165dupA	p.(Ser389LysfsTer2)	0
			Splicing variants			
518	LCA	heterozygous	exon2	c.86–1G>A	none	1.07E-05
1275	LCA	heterozygous	exon2	c.86–1G>A	none	1.07E-05
FBP_207	RP	heterozygous	exon14	c.1763–2A>G	none	1.07E-05

Table 2. Solved cases and Unsolved cases of IRD.

Disease	Total	LCA	RP
Solved cases	1450	375	1075
Cases solved by *RPGRIP1* biallelic mutations	37	26	11
Unsolved cases	933	171	762
Unsolved *RPGRIP1* one-hit cases	25	10	15
Expected case		2.31	14.86
Binomial test p value (one sided)		1.26E-04	0.52

Table 3. One deletion mutation and two deep intronic cryptic splicing mutation identified in this study.

Patient ID[a]	Clinical diagnosis	First allele [b]			Second allele [c]				Segregation available
		zygosity	cDNA variant	gnomAD (Allele frequency)	Protein variant	cDNA variant	gnomAD (Allele frequency)	Protein variant	SpliceAI Score	
MEP_305	LCA	heterozygous	c.3793_3794insGAAA	4.04E-06	p.(Val1265GlyfsTer19)	c.2710+233G>A	0	intronic	0.66	NO
MEP_318	LCA	heterozygous	c.934dupC	0	p.(Gln312ProfsTer9)	c.1468–263G>C	0	intronic	0.39	NO
RKK_665	LCA	heterozygous	c.2627A>G	0	p.(Asp876Gly)	c.3340_c.3533del2890	0	p.(Ala1113_Lys1177delfs*(64))		NO

[a]Patient IDs are from Casey Eye Institute Oregon Health & Science University. Family numbers follows the individual patient number.[b]*RPGRIP1* alleles that presented the unsolved one-hit data are identified from previous WES results. [c] The second allele shown is included in validation assay.

21,809,977 and 21,812,868, resulting in a deletion of 2,890 bp in length. As a result, the entire exon 21 of *RPGRIP1* was deleted. As exon 21 is 193 bp, deletion of the exon would lead to a reading frameshift and likely trigger nonsense-mediated mRNA decay (NMD), resulting in a complete loss of function mutation.

The clinical phenotype of the proband (RKK_665) is a 44-year-old female with LCA. She first presented at age 4 years with congenital nystagmus, visual defects including poor night vision, and marked light sensitivity. Her BCVA decreased to 20/240 for both eyes. As shown in Figure 3C, fundus examination of both eyes showed optic disc pallor (mild) and diffuse retinal pigmentation and atrophy with arteriolar narrowing. OCT examination showed thinning of the retina and a small remaining subfoveal ellipsoid zone (EZ) in the right eye (Figure 3D). She did not complain of visual field defects, although her superior peripheral visual field showed defects (Figure 3E).

DISCUSSION

A significant proportion of patients with IRDs currently remain unexplained upon exon capture sequencing in the known IRD-associated genes. Noncoding mutations and structural variation of the disease genes have been shown to contribute to the disease burden. The carrier frequency in coding regions of some IRD genes is higher in patients with unsolved IRDs than expected. These observations suggest that these carriers are enriched with noncoding variants and structure mutations that are missed by current WES or panel sequencing. To test this hypothesis, we systematically

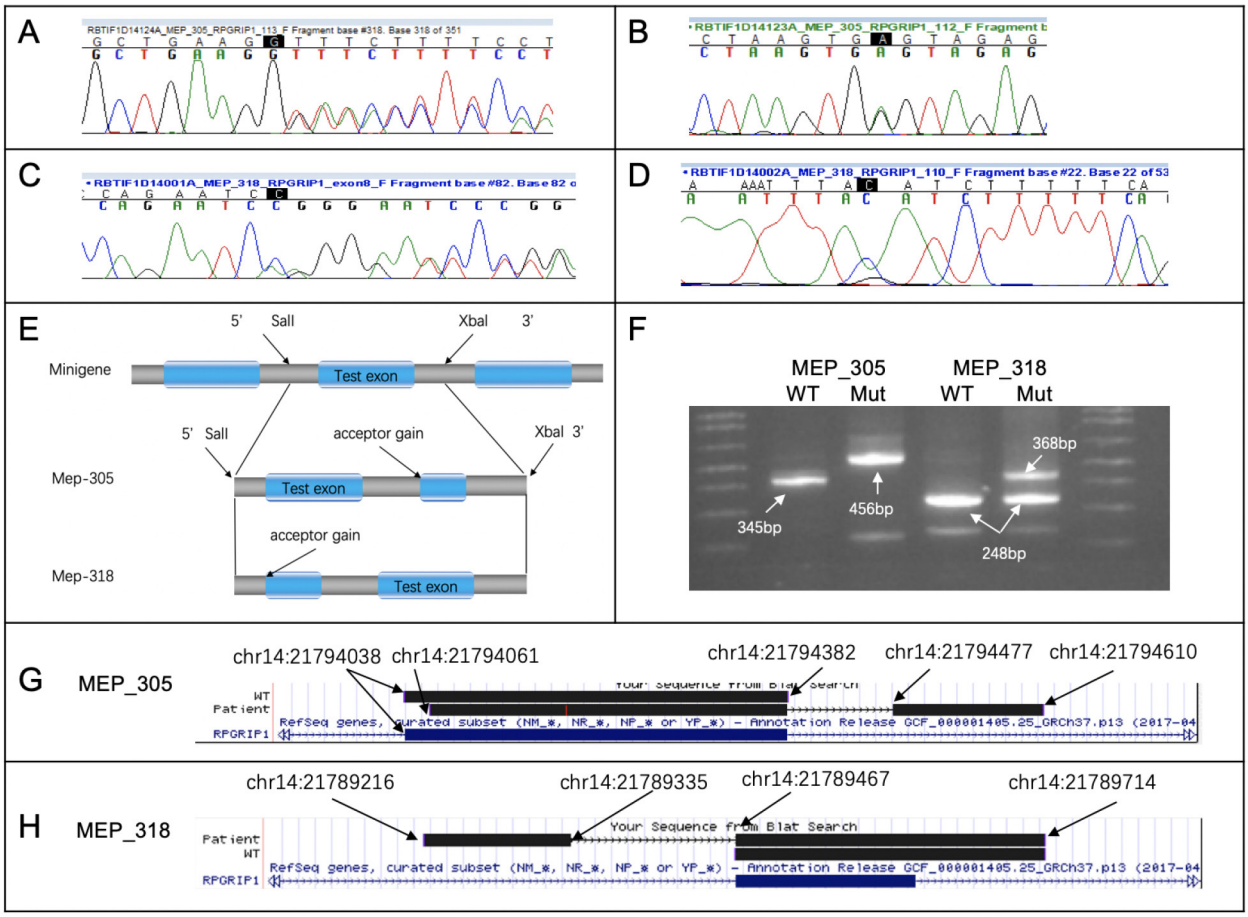

Figure 2. Validation of two cryptic splicing mutation alleles. Validation of two cryptic splicing mutation alleles. Sanger sequencing verified (**A**) the coding mutation (c.3793_3794insGAAA) and (**B**) the deep-intronic mutation (c.2710+233G>A) in MEP_305, (**C**) the coding mutation (c.934dupC), and (**D**) the deep-intronic mutation (c.1468–263G>C) in MEP_318. **E**: Schematic drawing of the minigene splicing assay. **F**: Using the minigene splicing assay, cryptic splicing induced by the two deep-intronic mutations is observed. Larger reverse transcriptase (RT)–PCR products are observed in the construct carrying the mutation compared to the wild-type control construct. **G**, **H**: Sanger sequencing of the RT–PCR band further confirms the splicing junction.

investigated noncoding variants and structure variations in *RPGRIP1*, a gene with a high number of carriers in the unsolved patient cohort. WGS identified three patients with a second mutant allele in *RPGRIP1*, including two deep-intronic splicing mutations and a large deletion. One of the two deep-intronic splicing mutations identified in this study, c.1468–263G>C, was reported previously while the other, c.2710+233G>A, is novel [33]. Although the identification of deep-intronic splicing variants has been challenging, the recently published SpliceAI appears to be effective in predicting such variants. In this study, two deep-intronic variants were predicted to result in donor splice-site gain and

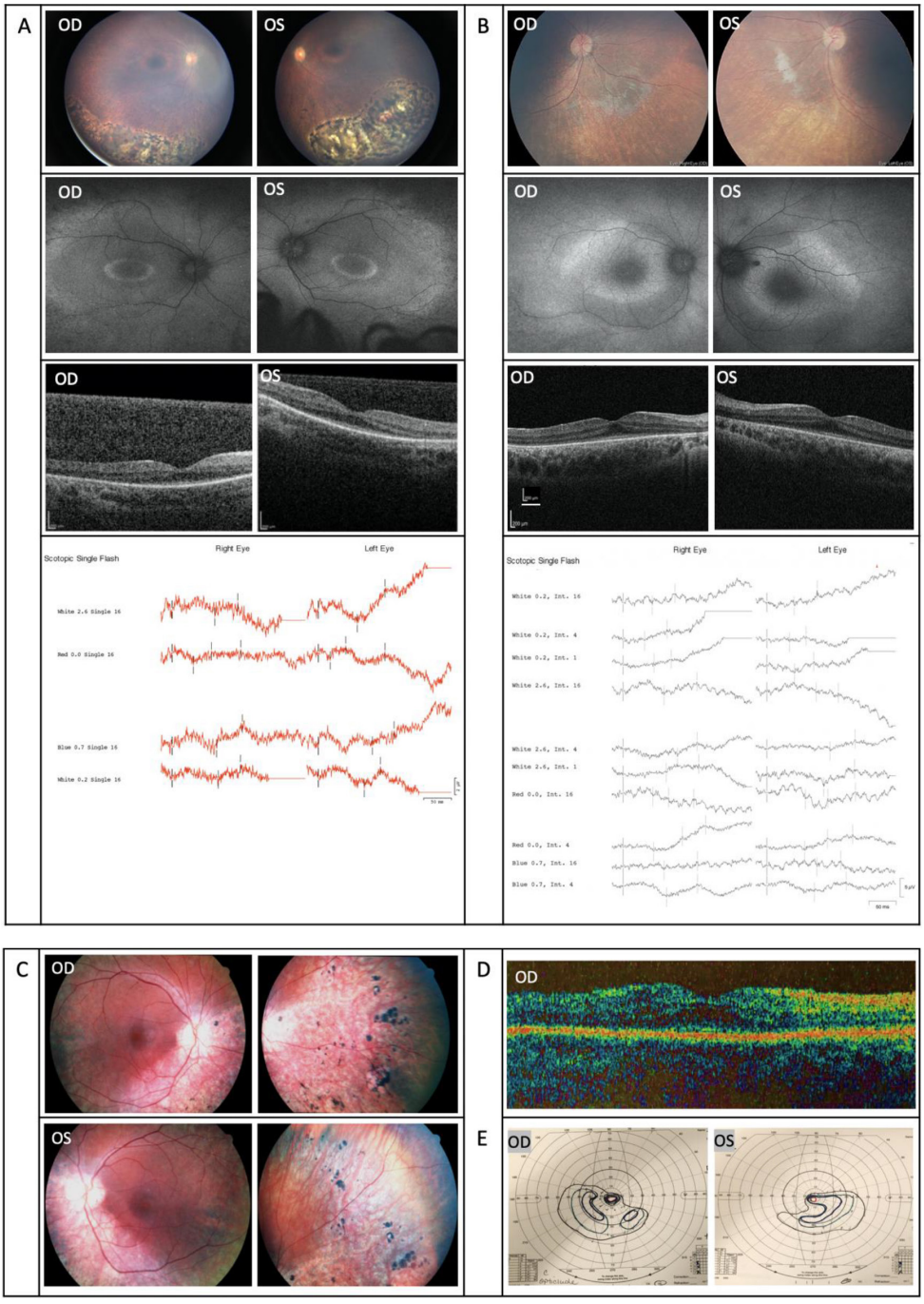

Figure 3. The clinical features of the individuals with LCA. **A**: Patient MEP-305. **B**: Patient MEP-318. The top row shows fundus imaging. The second row shows autofluorescence (AF) imaging. The third row shows optical coherence tomography (OCT) imaging. The bottom row shows full-field electroretinography (ffERG). In patient A, there are vascular attenuation, RPE atrophy with increased visibility of choroidal vessels, and fine granular pigmentation just outside the vessels. The pigmentary changes inferiorly are secondary to laser for a Coats-like reaction that the patient developed. AF imaging showed a perimacular hyper-AF ring. In patient B, the fundus of both eyes indicates moderate waxy pallor, mottling in macula, as well as moderate vascular attenuation. AF imaging shows peripheral hypo-AF and hyper-AF rings of the parafovea and midperiphery OU. The ffERG of patients A and B reveals severe cone and rod dysfunction. OCT imaging shows that the two patients have a relatively normal foveal structure. **C**–**E**: Phenotypes of patient RKK_665. **C**: Retinal photographs of both eyes illustrating optic disc pallor and diffuse retinal pigmentation and atrophy with arteriolar narrowing but much more pronounced inferiorly in both eyes. This corresponds to the absence of Goldmann visual fields superiorly OU. In the periphery, there are marked nummular pigmented clumps and areas of atrophy. **D**: Thinning of the retina and a small remaining subfoveal ellipsoid zone (EZ), illustrating the remaining photoreceptors, likely cones. **E**: Significant remaining central and inferior field in both eyes. The superior visual fields are absent in both eyes.

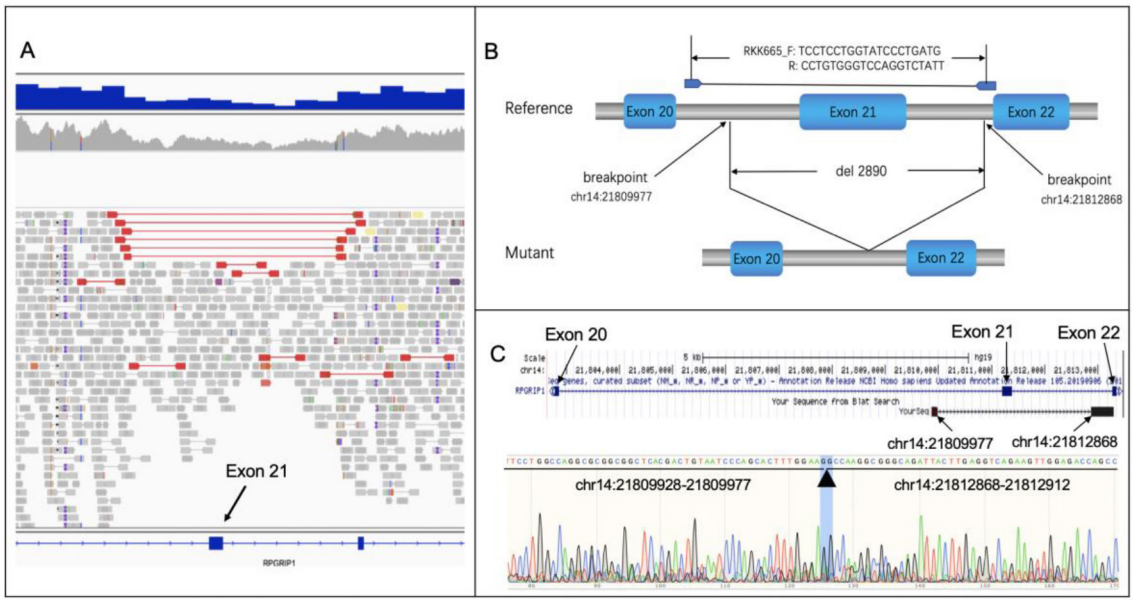

Figure 4. RKK_665 carries a deletion mutation. **A**: Integrative Genomics Viewer (IGV) view of the sequenced genome sequencing (GS) reads the location of the deletion in the RKK_665 patient. The bottom shows the location of exon 21 and exon 22 in *RPGRIP1*. The gray thick arrows correspond to the expected paired end reads. The thick red arrows are mapped reads that have aligned abnormally and represent a deletion. **B**: Schematic plot explains the 2,890-bp deletion in the RKK_665 patient. The primers for Sanger sequencing of the deletion are listed in the top (RKK665_F: left primer, _R: right primer). **C**: Junction PCR was conducted (with the primers listed in **B**), and the PCR product was Sanger sequenced. The top is the BLAT alignment of the Sanger sequencing product against the hg19 human genome, which confirmed the 2,890-bp deletion, the breakpoints (chr14:21809977 and chr14:21812868), and the absence of exon 21, as shown in the UCSC Genome Browser. The bottom shows the Sanger sequencing data identifying the exact breakpoints (black arrowhead).

aberrant splicing with new exon gain. Both predictions were experimentally confirmed with the minigene test.

Despite improved detection of pathogenic variants with WGS, SVs remain difficult to identify due to limitations of short-read sequencing in identifying breakpoints. By combining multiple software predictions for SVs and CNVs, we identified a structural variation that causes an aberrant reading frame as the second pathogenic allele in RKK_665. By sequencing the PCR products of the large deletion and aligning it with the reference sequence, we validated the deletion with a breakpoint at c.3340_c.3533del2890. This finding indicates that deletions in *RPGRIP1* could explain some unsolved one-hit *RPGRIP1* cases and suggests screening of SVs may be necessary to explain the patients with unsolved IRDs.

After we identified pathogenic alleles in noncoding regions and SVs, one hit of *RPGRIP1* remained enriched in the unsolved LCA cohort, implying that there may be second hits that remain undetected. In contrast, one hit of *RPGRIP1* was not significantly more frequent in this RP cohort. This might be because mutations in *RPGRIP1* account for fewer than 2% of patients with RP [43-49]. Overall, the study results indicate that it is important to thoroughly investigate SVs and noncoding variations to identify the missing mutations in unsolved cases with a higher priority for IRD genes with higher carrier frequency in coding regions than expected in patients with unsolved IRDs.

APPENDIX 1. STR ANALYSIS

STR analysis of HEK293 cell line. To access the data, click or select the words "Appendix 1."

ACKNOWLEDGMENTS

We thank the patients and families for their enthusiastic participation. We thank Iris Chen for reading and editing the manuscript. This work is supported by the key research and development program Ningxia Hui Autonomous Region of China (2020BEG03044) to GZ, CIHR, Fighting Blindness Canada, MCH Foundation and Reseau de Vision to RKK, Retinal Research Foundation to RC. Dr. GAF acknowledges funding from the Pangere family. NIH K08EY026650 to PY. Supported by grant P30EY010572 from the National Institutes of Health (Bethesda, MD), and by unrestricted

departmental funding from Research to Prevent Blindness (New York, NY).

REFERENCES

1. Ellingford JM, Barton S, Bhaskar S, Sullivan J, Williams SG, Lamb JA, Panda B, Sergouniotis PI, Gillespie RL, Daiger SP, Hall G, Gale T, Lloyd IC, Bishop PN, Ramsden SC, Black GCM. Molecular findings from 537 individuals with inherited retinal disease. J Med Genet 2016; 53:761-[PMID: 27208204].
2. Lee K, Berg JS, Milko L, Crooks K, Lu M, Bizon C, Owen P, Wilhelmsen KC, Weck KE, Evans JP. High diagnostic yield of whole exome sequencing in participants with retinal dystrophies in a clinical ophthalmology setting. Am J Ophthalmol 2015; 160:354-63. .
3. Wang H, Wang X, Zou X, Xu S, Li H, Soens ZT, Wang K, Li Y, Dong F, Chen R. Comprehensive molecular diagnosis of a large Chinese Leber congenital amaurosis cohort. Invest Ophthalmol Vis Sci 2015; 56:3642-55. [PMID: 26047050].
4. O'Sullivan J, Mullaney BG, Bhaskar SS, Dickerson JE, Hall G, O'Grady A, Webster A, Ramsden SC, Black GC. A paradigm shift in the delivery of services for diagnosis of inherited retinal disease. J Med Genet 2012; 49:322-6. [PMID: 22581970].
5. Coppieters F, Casteels I, Meire F, De Jaegere S, Hooghe S, Van Regemorter N, Van Esch H, Matulevičienė A, Nunes L, Meersschaut V. Genetic screening of LCA in Belgium: predominance of CEP290 and identification of potential modifier alleles in AHI1 of CEP290-related phenotypes. Hum Mutat 2010; 31:E1709-66. [PMID: 20683928].
6. den Hollander AI, Koenekoop RK, Yzer S, Lopez I, Arends ML, Voesenek KE, Zonneveld MN, Strom TM, Meitinger T, Brunner HG. Mutations in the CEP290 (NPHP6) gene are a frequent cause of Leber congenital amaurosis. Am J Hum Genet 2006; 79:556-61. [PMID: 16909394].
7. Perrault I, Delphin N, Hanein S, Gerber S, Dufier JL, Roche O, Defoort-Dhellemmes S, Dollfus H, Fazzi E, Munnich A. Spectrum of NPHP6/CEP290 mutations in Leber congenital amaurosis and delineation of the associated phenotype. Hum Mutat 2007; 28:416-[PMID: 17345604].
8. Vallespin E, Lopez-Martinez M-A, Cantalapiedra D, Riveiro-Alvarez R, Aguirre-Lamban J, Avila-Fernandez A, Villaverde C, Trujillo-Tiebas M-J, Ayuso C. Frequency of CEP290 c. 2991_1655A> G mutation in 175 Spanish families affected with Leber congenital amaurosis and early-onset retinitis pigmentosa. Mol Vis 2007; 13:2160-2. [PMID: 18079693].
9. Bax NM, Sangermano R, Roosing S, Thiadens AA, Hoefsloot LH, van den Born LI, Phan M, Klevering BJ, Westeneng-van Haaften C, Braun TA, Zonneveld-Vrieling MN, de Wijs I, Mutlu M, Stone EM, den Hollander AI, Klaver CC, Hoyng CB, Cremers FP. Heterozygous deep-intronic variants and deletions in ABCA4 in persons with retinal dystrophies and one exonic ABCA4 variant. Hum Mutat 2015; 36:43-7. [PMID: 25363634].
10. Schulz HL, Grassmann F, Kellner U, Spital G, Rüther K, Jägle H, Hufendiek K, Rating P, Huchzermeyer C, Baier MJ, Weber BHF, Stöhr H. Mutation Spectrum of the ABCA4 Gene in 335 Stargardt Disease Patients From a Multicenter German Cohort-Impact of Selected Deep Intronic Variants and Common SNPs. Invest Ophthalmol Vis Sci 2017; 58:394-403. [PMID: 28118664].
11. Sangermano R, Garanto A, Khan M, Runhart EH, Bauwens M, Bax NM, van den Born LI, Khan MI, Cornelis SS, Verheij JBGM, Pott J-WR, Thiadens AAHJ, Klaver CCW, Puech B, Meunier I, Naessens S, Arno G, Fakin A, Carss KJ, Raymond FL, Webster AR, Dhaenens C-M, Stöhr H, Grassmann F, Weber BHF, Hoyng CB, De Baere E, Albert S, Collin RWJ, Cremers FPM. Deep-intronic ABCA4 variants explain missing heritability in Stargardt disease and allow correction of splice defects by antisense oligonucleotides. Genet Med 2019; 21:1751-60. [PMID: 30643219].
12. Zernant J, Lee W, Nagasaki T, Collison FT, Fishman GA, Bertelsen M, Rosenberg T, Gouras P, Tsang SH, Allikmets R. Extremely hypomorphic and severe deep intronic variants in the ABCA4 locus result in varying Stargardt disease phenotypes. Cold Spring Harb Mol Case Stud 2018; 4:a002733-[PMID: 29848554].
13. Bauwens M, De Zaeytijd J, Weisschuh N, Kohl S, Meire F, Dahan K, Depasse F, De Jaegere S, De Ravel T, De Rademaeker M. An Augmented ABCA 4 Screen Targeting Noncoding Regions Reveals a Deep Intronic Founder Variant in B elgian S targardt Patients. Hum Mutat 2015; 36:39-42. [PMID: 25346251].
14. Khan M, Cornelis SS, Khan MI, Elmelik D, Manders E, Bakker S, Derks R, Neveling K, van de Vorst M, Gilissen C, Meunier I, Defoort S, Puech B, Devos A, Schulz HL, Stöhr H, Grassmann F, Weber BHF, Dhaenens C-M, Cremers FPM. Cost-effective molecular inversion probe-based ABCA4 sequencing reveals deep-intronic variants in Stargardt disease. Hum Mutat 2019; 40:1749-59. [PMID: 31212395].
15. Zernant J, Xie YA, Ayuso C, Riveiro-Alvarez R, Lopez-Martinez MA, Simonelli F, Testa F, Gorin MB, Strom SP, Bertelsen M, Rosenberg T, Boone PM, Yuan B, Ayyagari R, Nagy PL, Tsang SH, Gouras P, Collison FT, Lupski JR, Fishman GA, Allikmets R. Analysis of the ABCA4 genomic locus in Stargardt disease. Hum Mol Genet 2014; 23:6797-806. [PMID: 25082829].
16. Braun TA, Mullins RF, Wagner AH, Andorf JL, Johnston RM, Bakall BB, Deluca AP, Fishman GA, Lam BL, Weleber RG, Cideciyan AV, Jacobson SG, Sheffield VC, Tucker BA, Stone EM. Non-exomic and synonymous variants in ABCA4 are an important cause of Stargardt disease. Hum Mol Genet 2013; 22:5136-45. [PMID: 23918662].
17. Duncker T, Tsang SH, Lee W, Zernant J, Allikmets R, Delori FC, Sparrow JR. Quantitative fundus autofluorescence distinguishes ABCA4-associated and non-ABCA4-associated bull's-eye maculopathy. Ophthalmology 2015; 122:345-55. [PMID: 25283059].
18. Fadaie Z, Khan M, Del Pozo-Valero M, Cornelis SS, Ayuso C, Cremers FPM, Roosing S. The Abca Study G. Identification

of splice defects due to noncanonical splice site or deep-intronic variants in ABCA4. Hum Mutat 2019; 40:2365-2376. .

19. Steele-Stallard HB, Le Quesne Stabej P, Lenassi E, Luxon LM, Claustres M, Roux A-F, Webster AR, Bitner-Glindzicz M. Screening for duplications, deletions and a common intronic mutation detects 35% of second mutations in patients with USH2A monoallelic mutations on Sanger sequencing. Orphanet J Rare Dis 2013; 8:122-[PMID: 23924366].

20. García-García G, Aller E, Jaijo T, Aparisi MJ, Larrieu L, Faugère V, Blanco-Kelly F, Ayuso C, Roux A-F, Millán JM. Novel deletions involving the USH2A gene in patients with Usher syndrome and retinitis pigmentosa. Mol Vis 2014; 20:1398-410. [PMID: 25352746].

21. Koenekoop RK. RPGRIP1 is mutated in Leber congenital amaurosis: a mini-review. Ophthalmic Genet 2005; 26:175-9. [PMID: 16352478].

22. Shu X, Black GC, Rice JM, Hart-Holden N, Jones A, O'Grady A, Ramsden S, Wright AF. RPGR mutation analysis and disease: an update. Hum Mutat 2007; 28:322-8. [PMID: 17195164].

23. Dryja TP, Adams SM, Grimsby JL, McGee TL, Hong D-H, Li T, Andréasson S, Berson EL. Null RPGRIP1 alleles in patients with Leber congenital amaurosis. Am J Hum Genet 2001; 68:1295-8. [PMID: 11283794].

24. Gerber S, Perrault I, Hanein S, Barbet F, Ducroq D, Ghazi I, Martin-Coignard D, Leowski C, Homfray T, Dufier J-L. Complete exon-intron structure of the RPGR-interacting protein (RPGRIP1) gene allows the identification of mutations underlying Leber congenital amaurosis. Eur J Hum Genet 2001; 9:561-71. [PMID: 11528500].

25. Booij JC, Florijn RJ, ten Brink JB, Loves W, Meire F, van Schooneveld MJ, de Jong PT, Bergen AA. Identification of mutations in the AIPL1, CRB1, GUCY2D, RPE65, and RPGRIP1 genes in patients with juvenile retinitis pigmentosa. J Med Genet 2005; 42:e67-.

26. Hameed A, Abid A, Aziz A, Ismail M, Mehdi S, Khaliq S. Evidence of RPGRIP1 gene mutations associated with recessive cone-rod dystrophy. J Med Genet 2003; 40:616-9. [PMID: 12920076].

27. Eblimit A, Nguyen TM, Chen Y, Esteve-Rudd J, Zhong H, Letteboer S, Van Reeuwijk J, Simons DL, Ding Q, Wu KM, Li Y, Van Beersum S, Moayedi Y, Xu H, Pickard P, Wang K, Gan L, Wu SM, Williams DS, Mardon G, Roepman R, Chen R. Spata7 is a retinal ciliopathy gene critical for correct RPGRIP1 localization and protein trafficking in the retina. Hum Mol Genet 2015; 24:1584-601. [PMID: 25398945].

28. Won J, Gifford E, Smith RS, Yi H, Ferreira PA, Hicks WL, Li T, Naggert JK, Nishina PM. RPGRIP1 is essential for normal rod photoreceptor outer segment elaboration and morphogenesis. Hum Mol Genet 2009; 18:4329-39. [PMID: 19679561].

29. Roepman R, Bernoud-Hubac N, Schick DE, Maugeri A, Berger W, Ropers HH, Cremers FP, Ferreira PA. The retinitis pigmentosa GTPase regulator (RPGR) interacts with novel transport-like proteins in the outer segments of rod photoreceptors. Hum Mol Genet 2000; 9:2095-105. [PMID: 10958648].

30. Hong DH, Yue G, Adamian M, Li T. Retinitis pigmentosa GTPase regulator (RPGRr)-interacting protein is stably associated with the photoreceptor ciliary axoneme and anchors RPGR to the connecting cilium. J Biol Chem 2001; 276:12091-9. [PMID: 11104772].

31. Murga-Zamalloa CA, Desai NJ, Hildebrandt F, Khanna H. Interaction of ciliary disease protein retinitis pigmentosa GTPase regulator with nephronophthisis-associated proteins in mammalian retinas. Mol Vis 2010; 16:1373-81. [PMID: 20664800].

32. Suzuki T, Fujimaki T, Yanagawa A, Arai E, Fujiki K, Wada Y, Murakami A. A novel exon 17 deletion mutation of RPGRIP1 gene in two siblings with Leber congenital amaurosis. Jpn J Ophthalmol 2014; 58:528-35. [PMID: 25096270].

33. Jamshidi F, Place EM, Mehrotra S, Navarro-Gomez D, Maher M, Branham KE, Valkanas E, Cherry TJ, Lek M, MacArthur D, Pierce EA, Bujakowska KM. Contribution of noncoding pathogenic variants to RPGRIP1-mediated inherited retinal degeneration. Genet Med 2019; 21:694-704. [PMID: 30072743].

34. Wang J, Liu H, Bertrand RE, Sarrion-Perdigones A, Gonzalez Y, Venken KJT, Chen R. A novel statistical method for interpreting the pathogenicity of rare variants. Genet Med 2020; 23:59-68. [PMID: 32884132].

35. Li H, Durbin R. Fast and accurate short read alignment with Burrows-Wheeler transform. Bioinformatics 2009; 25:1754-60. [PMID: 19451168].

36. Kircher M, Witten DM, Jain P, O'Roak BJ, Cooper GM, Shendure J. A general framework for estimating the relative pathogenicity of human genetic variants. Nat Genet 2014; 46:310-5. [PMID: 24487276].

37. Rentzsch P, Witten D, Cooper GM, Shendure J, Kircher M. CADD: predicting the deleteriousness of variants throughout the human genome. Nucleic Acids Res 2019; 47:D1D886-94. [PMID: 30371827].

38. Xu M, Xie YA, Abouzeid H, Gordon CT, Fiorentino A, Sun Z, Lehman A, Osman IS, Dharmat R, Riveiro-Alvarez R, Bapst-Wicht L, Babino D, Arno G, Busetto V, Zhao L, Li H, Lopez-Martinez MA, Azevedo LF, Hubert L, Pontikos N, Eblimit A, Lorda-Sanchez I, Kheir V, Plagnol V, Oufadem M, Soens ZT, Yang L, Bole-Feysot C, Pfundt R, Allaman-Pillet N, Nitschke P, Cheetham ME, Lyonnet S, Agrawal SA, Li H, Pinton G, Michaelides M, Besmond C, Li Y, Yuan Z, von Lintig J, Webster AR, Le Hir H, Stoilov P, Consortium UKIRD, Amiel J, Hardcastle AJ, Ayuso C, Sui R, Chen R, Allikmets R, Schorderet DF. Mutations in the Spliceosome Component CWC27 Cause Retinal Degeneration with or without Additional Developmental Anomalies. Am J Hum Genet 2017; 100:592-604. [PMID: 28285769].

39. Chiang C, Layer RM, Faust GG, Lindberg MR, Rose DB, Garrison EP, Marth GT, Quinlan AR, Hall IM. SpeedSeq: ultra-fast personal genome analysis and interpretation. Nat Methods 2015; 12:966-8. [PMID: 26258291].

40. Ebler J, Schonhuth A, Marschall T. Genotyping inversions and tandem duplications. Bioinformatics 2017; 33:4015-23. [PMID: 28169394].

41. Jaganathan K, Kyriazopoulou Panagiotopoulou S, McRae JF, Darbandi SF, Knowles D, Li YI, Kosmicki JA, Arbelaez J, Cui W, Schwartz GB, Chow ED, Kanterakis E, Gao H, Kia A, Batzoglou S, Sanders SJ, Farh KK-H. Predicting Splicing from Primary Sequence with Deep Learning. Cell 2019; 176:535-48.e24. [PMID: 30661751].

42. Soens ZT, Branch J, Wu S, Yuan Z, Li Y, Li H, Wang K, Xu M, Rajan L, Motta FL, Simões RT, Lopez-Solache I, Ajlan R, Birch DG, Zhao P, Porto FB, Sallum J, Koenekoop RK, Sui R, Chen R. Leveraging splice-affecting variant predictors and a minigene validation system to identify Mendelian disease-causing variants among exon-captured variants of uncertain significance. Hum Mutat 2017; 38:1521-33. [PMID: 28714225].

43. Huang H, Wang Y, Chen H, Chen Y, Wu J, Chiang PW, Fan N, Su Y, Deng J, Chen D, Li Y, Zhang X, Zhang M, Liang S, Banerjee S, Qi M, Liu X. Targeted next generation sequencing identified novel mutations in RPGRIP1 associated with both retinitis pigmentosa and Leber's congenital amaurosis in unrelated Chinese patients. Oncotarget 2017; 8:35176-83. [PMID: 28456785].

44. Birtel J, Gliem M, Mangold E, Muller PL, Holz FG, Neuhaus C, Lenzner S, Zahnleiter D, Betz C, Eisenberger T, Bolz HJ, Charbel Issa P. Next-generation sequencing identifies unexpected genotype-phenotype correlations in patients with retinitis pigmentosa. PLoS One 2018; 13:e0207958-[PMID: 30543658].

45. Ge Z, Bowles K, Goetz K, Scholl HP, Wang F, Wang X, Xu S, Wang K, Wang H, Chen R. NGS-based Molecular diagnosis of 105 eyeGENE((R)) probands with Retinitis Pigmentosa. Sci Rep 2015; 5:18287-[PMID: 26667666].

46. Zhao L, Wang F, Wang H, Li Y, Alexander S, Wang K, Willoughby CE, Zaneveld JE, Jiang L, Soens ZT, Earle P, Simpson D, Silvestri G, Chen R. Next-generation sequencing-based molecular diagnosis of 82 retinitis pigmentosa probands from Northern Ireland. Hum Genet 2015; 134:217-30. [PMID: 25472526].

47. Wang F, Wang H, Tuan HF, Nguyen DH, Sun V, Keser V, Bowne SJ, Sullivan LS, Luo H, Zhao L, Wang X, Zaneveld JE, Salvo JS, Siddiqui S, Mao L, Wheaton DK, Birch DG, Branham KE, Heckenlively JR, Wen C, Flagg K, Ferreyra H, Pei J, Khan A, Ren H, Wang K, Lopez I, Qamar R, Zenteno JC, Ayala-Ramirez R, Buentello-Volante B, Fu Q, Simpson DA, Li Y, Sui R, Silvestri G, Daiger SP, Koenekoop RK, Zhang K, Chen R. Next generation sequencing-based molecular diagnosis of retinitis pigmentosa: identification of a novel genotype-phenotype correlation and clinical refinements. Hum Genet 2014; 133:331-45. [PMID: 24154662].

48. Fu Q, Wang F, Wang H, Xu F, Zaneveld JE, Ren H, Keser V, Lopez I, Tuan HF, Salvo JS, Wang X, Zhao L, Wang K, Li Y, Koenekoop RK, Chen R, Sui R. Next-generation sequencing-based molecular diagnosis of a Chinese patient cohort with autosomal recessive retinitis pigmentosa. Invest Ophthalmol Vis Sci 2013; 54:4158-66. [PMID: 23661369].

49. Zhang Q, Xu M, Verriotto JD, Li Y, Wang H, Gan L, Lam BL, Chen R. Next-generation sequencing-based molecular diagnosis of 35 Hispanic retinitis pigmentosa probands. Sci Rep 2016; 6:32792-[PMID: 27596865].

Articles are provided courtesy of Emory University and the Zhongshan Ophthalmic Center, Sun Yat-sen University, P.R. China. The print version of this article was created on 18 March 2021. This reflects all typographical corrections and errata to the article through that date. Details of any changes may be found in the online version of the article.